The New Generation of the KIT 3D USCT

H. Gemmeke, L. Berger, T. Hopp, M. Zapf, W. Tan, R. Blanco, R. Leys, I. Peric, and N. Ruiter

Karlsruhe Institute of Technology, Karlsruhe, Germany
E-mail: hartmut.gemmeke@kit.edu

Abstract

The first clinical studies with our current prototype, 3D USCT II, enabled us to identify the necessary improvements for transition of our method to clinical practice. The main goals are to improve the contrast of reflection and transmission tomography, and to optimize the coverage of the imaged breast by a new geometry of the transducer distribution. Furthermore, for cost-effective industrial mass production, a self-calibration method allows us to relax the precision of the positioning of the transducers to 0.1 mm. The readout of the transducer arrays is now carried out by an ASIC, developed for a more cost-effective design. The coupling of the measuring device to the patient was optimized to cover the full size of the breast up to the pectoral muscles. Finally, the data acquisition and readout time were reduced to 1.5 minutes each by new micro-TCA electronics and larger FPGAs.

Keywords: breast cancer, medical imaging, reflection tomography, transmission tomography

1   Introduction

Our 3D Ultrasound Computer Tomography system for breast imaging [1] is shown in Fig. 1. It consists of a patient bed with an embedded ellipsoidal measuring device covered by 2041 transducers contained in 157 transducer arrays (TAS) [2]. The ellipsoidal aperture has a diameter of 26 cm and a depth of 18 cm. The coupling medium is water at body temperature. Using 10 million A-scans, which describe the pressure over time, we could reconstruct 3D reflectivity images of the breast with sub-millimeter resolution using synthetic aperture technique [3]. The speed-of-sound and attenuation were reconstructed from the same raw data set by a straight ray based algebraic reconstruction technique [4]. The necessary fast data acquisition (DAQ) electronics was adapted from our development for the cosmic ray experiment AUGER [5].

Figure 1: KIT 3D USCT with look in the inner structure (left) and transducer aperture (right).

At the University Hospital Jena we carried out a pilot study with the prototype, 3D USCT II, which enabled us to identify the necessary improvements for transition of our method to clinical practice. The main goals are:

1. Improvement of the contrast in reflection and transmission tomography by a new geometry of the transducer distribution. A uniform random distribution of transducers may minimize the artifacts of the sparse aperture and maximize the contrast in the reconstructed images.
2. The interface of the measuring device to the patient should be optimized to cover the full size of the breast up to the pectoral muscles.
3. A further aim was to enlarge the aperture for better immersion of large breasts into the device.
4. Finally, the DAQ and readout time should be reduced by a new electronic.

The strategy of development, the steps of optimization of geometry, their improvements to reflection and transmission tomography and the produced measuring device are described in the following sections. Furthermore, the new frontend ASIC for driving and receiving the ultrasound signals and the new data acquisition electronics are introduced and finally the so far obtained results discussed.

2 Strategy of Development

To lower the risk in the overall development we carry out the implementation in two steps. Starting from the current measuring system 3D USCT II with 157 TAS with 4 emitters and 9 receivers each, we test the production technology of a new transducer array system [6].
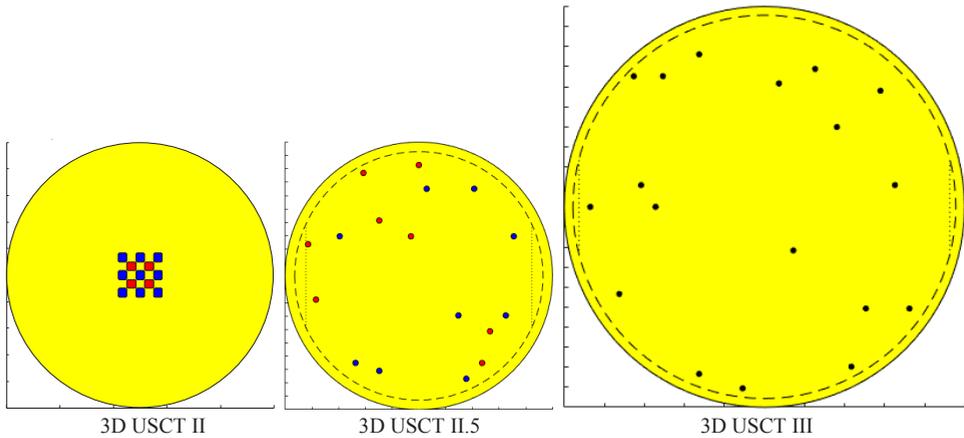
Figure 2: Distribution of transducer at 3D USCT II, II.5 and III displayed in the same scale. Red describes the emitter and blue the receivers. Whereas the TAS of USCT II and II.5 have the same diameter of 28 mm, the TAS of 3D USCT III has a diameter of 43 mm and its transducer (black) are operated omnidirectional.

The three types of TAS for 3D USCT II, II.5 and III are shown in Fig. 2. Due to the omni-directional characteristic of the transducers in 3D USCT III, the obtained number of A-scans per used transducers quadruplicate and the number of aperture positions (AP) could be reduced by the same scale. For a sufficient contrast and resolution about 1e7 A-scans are required. Whereas for 1e7 A-scans with 3D USCT II 10 APs are necessary, this number is reduced for 3D USCT II.5 to 5 APs and for 3D USCT III to 2 APs, thereby reducing the time-consuming aperture movements and minimizing the DAQ time from 6 to 4 and 2 minutes respectively.

The size of the aperture with 26 cm is to small to cover breasts of 20 cm diameter with limited opening angles of the transducers and to achieve a constant point-spread-function over the size of the breasts. Especially the boyancy in the water enlarges the horizontal diameters for fatty breasts. Based on simulations we choose an diameter of 36 cm for 3D USCT III.

3   Optimal Geometry of Measuring System

For a globally uniform distribution of transducer on the surface of the measuring device the TAS have to be spaced as tightly as possible, i.e. the area of the surface not covered by TAS has to be as small as possible. The aim was to increase the density of coverage with trans-ducer arrays from 75% in 3D USCT II to 80% in 3D USCT III.

3.1 Minimize holes in coverage

Covering a sphere or ellipsoid with circles is an old unsolved mathematical problem, named Thomson's problem [7]. Numerically it may be approximated by minimizing the energy of Coulomb charges on the surface of the measuring device. In the case of a half-sphere or semi-ellipsoid an effective method is to fill the surface row by row starting from the bottom. This method of optimization of TAS distribution was described in a patent application [8]. It starts with a fixed size of the measuring device and varies the size and number of TAS per row, places them as dense as possible and ascends to the next row. For fine tuning, the radius of the measuring device is varied until the predetermined number of TAS is reached and the efficiency of coverage is maximized.

3.2 Global uniform random distribution of transducers

We optimized possible transducer distributions using Monte Carlo simulations in respect to contrast, coverage of the region of interest (hemisphere of 20 cm diameter), and minimization of artifacts. For a cost-effective industrial mass production, the TAS design should be identical for each TAS. To achieve a global uniform random distribution of the transducers and avoiding constant angle differences between the transducers, the TAS can be rotated randomly. Scoring the uniform randomness, the surface was subdivided into equal areas and the frequency distribution of the hits in these areas by the position of the transducers was analyzed by a chi-square test similarly to the test of uniform random number generators [9].
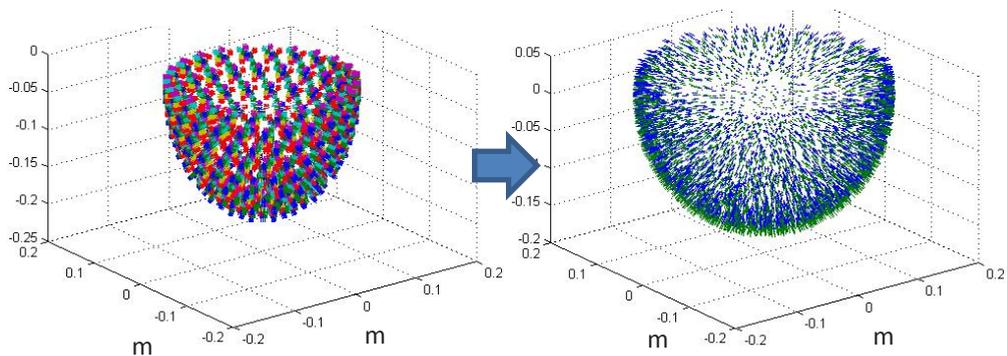
Figure 3: Transducer distribution in USCT II (left) with 12 APs and USCT III (right) with 2 APs.

The improvement in the distribution of transducers from 3D USCT II to 3D USCT III can be easily seen in Fig. 3. For one aperture position, a more uniform distribution without using the non-omnidirectional character of the transducer in 3D USCT II was obtained. To achieve a fair comparison, we use in both simulations the same number of A-scans.

4   Results

4.1   Contrast improvement in reflection tomography

Due to speed-of-sound correction we were able to achieve sub-wavelength resolution for reflection tomography with phantoms. Scattering and refraction does not significantly decrease resolution in the used frequency range of 2.5 MHz [10]. Yet, the contrast in reflection tomography is limited as we apply sparse array imaging. The artifacts, i.e. grating lobes, arise due to regular sampling at two orders of magnitude below the Nyquist limit, see Fig. 4 left, obtained with 900 000 A-scans or 1 AP with 3D USCT II. The artifacts can be reduced by a uniform random distribution of the transducers, see Fig. 4 right. By selection of 900 000 A-scans out of 10 APs with a uniform distribution of emitter and receiver, the grating lobes are greatly reduced. The same improvement we observed after increasing the number of APs to 22 [11]. Similar effects were observed at 2D sparse arrays [12].
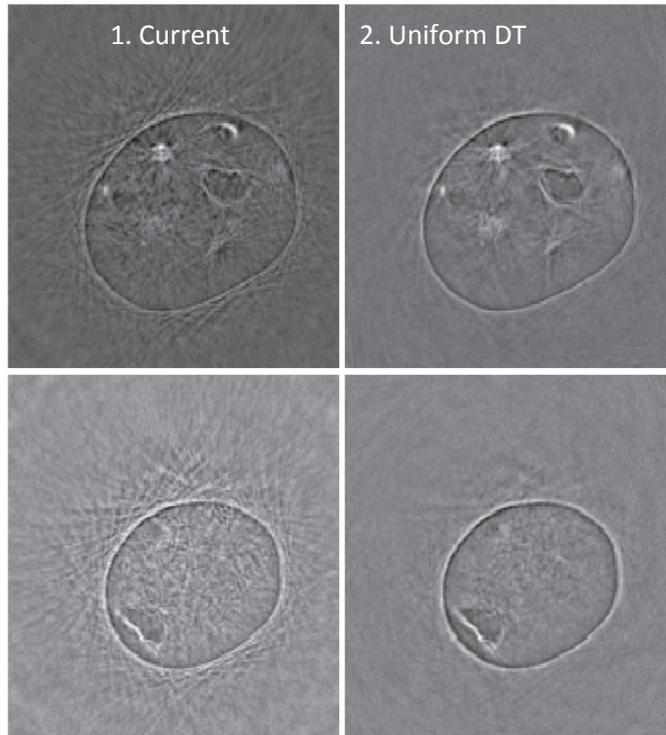
Figure 4:   Increasing contrast in reflection tomography from left to right by a more uniform distribution of transducers (DT). The number of A-scans is in both cases the same.

4.2   Improvement of transmission tomography

We tested the improvements on transmission tomography by a straight ray simulation for 3D USCT II and II.5 including the characteristics and distribution of the transducers and added noise. The simulated phantom (with a gradient of c = 1460 to 1500 m/s) is embedded in water (c = 1530 m/s) and contains eight lesions with a diameter of 5 to 12 mm testing the resolution, and seven lesions with a diameter of 10 mm and c = 1475 to 1560 m/s testing the contrast. The results are shown in Fig. 5. The reconstructed image with the 3D USCT II setup in Fig. 5b does not clearly depict the outline of the phantom for 1AP, but gives a more reasonable result at 16 AP in Fig. 5c. A reconstruction, Fig. 5d, with a 15° larger opening angle, ±35°, solves this problem, but still the contrast is low. Less clustering of the transducers results in a visibility of most test lesions in Fig. 5e still at 1 AP.
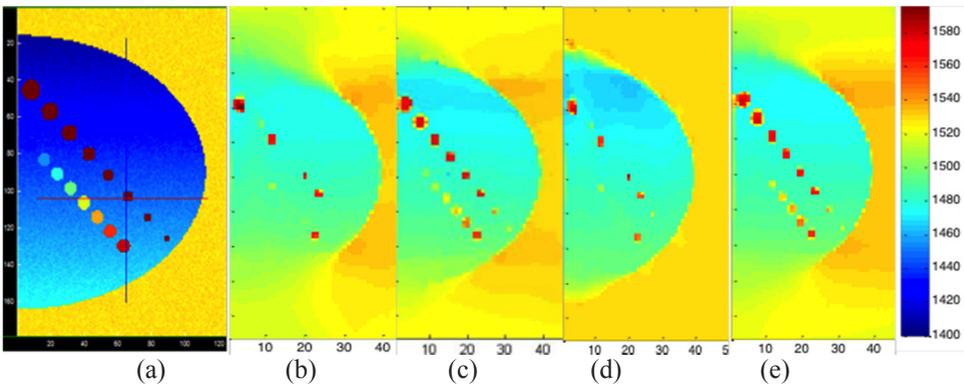
Figure 5:   3D simulation of a phantom (a) and reconstruction for 3D USCT II with different transducer distributions and parameters. 3D USCT II with 1 AP (b) and 16 AP (c), about 15° larger opening angles 1 AP (d) and 1 AP but uniform transducer distribution (e).

4.3   Final new aperture

Following these simulations, we choose for 3D USCT III a larger opening angle for the transducers and an enlarged aperture with a diameter of 36 cm (3D USCT II has 26 cm). By these changes we enlarge the field of view and depth of field from a diameter of 10 cm to 15 cm and 20 cm in version II.5 and III, respectively.

Due to the design, which allows vertical displacements of the measuring device, we lost in USCT 3D II 25 mm of the measuring range to the pectoralis, see Fig. 6 (right). By a new construction for 3D USCT III with a membrane (Fig. 6 left) we allow the same stroke of about 20 mm but reduce the losses to 5 mm. A small dead zone is acceptable, because tissue out of plane can also be reconstructed due to refraction and forward scattering.
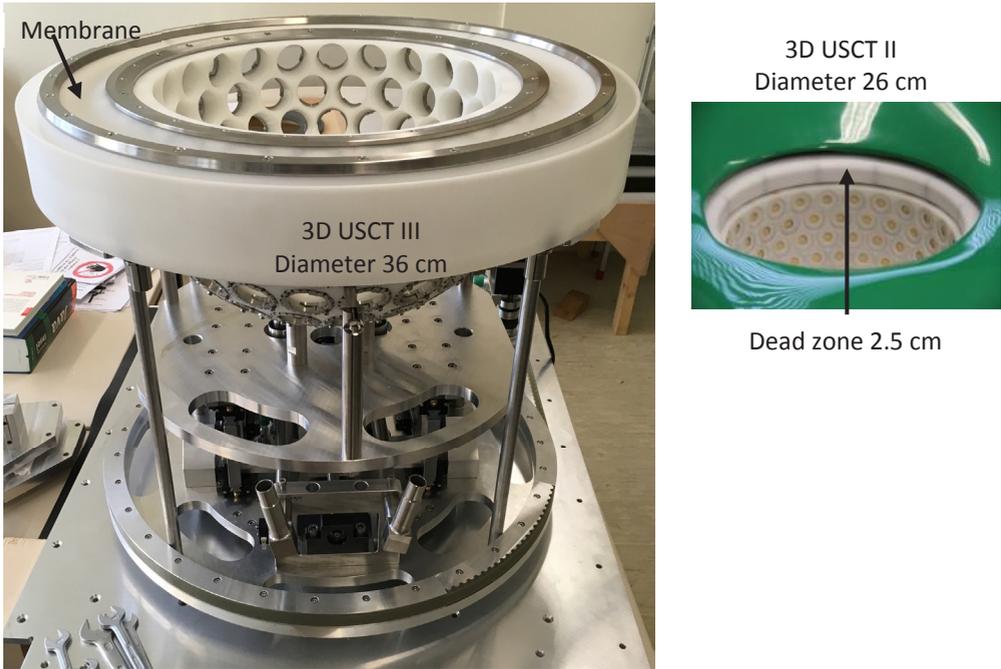
Figure 6: Hemispherical measuring device of 3D USCT III with 128 TAS (left) and the same for 3D USCT II with 157 TAS (right).

Furthermore, the transducers can be mounted under distinct different rotation angles and thus allows a better approximation of the uniform random distribution of transducers. Using all these provisions the simulations predicted relative improvements as described in Tab 1.

Ratio of new to current aperture			
Transmission-		Reflection-Tomography	
Resolution	2.0	Variability PSF	3.0
Contrast	3.0	Contrast	6.8
Visibility	2.3	Illumination	2.0

Table 1: Relative comparison of the quality of 3D USCT II and expected quality of 3D USCT III as extracted from simulations described in chapter 4.1 and 4.2.

4.4 New calibration method

The mechanical parts for the measuring device are machined with a precision of 20 microns to ensure positioning of the transducers with this accuracy. That is not a precision, which is standard for industrial mass production. Therefore, we developed a method to calibrate the position of transducers [13]. To test the method, we measured a sphere of stainless steel of diameter 50 mm, see Fig. 7a, which was fabricated with a precision of 50 µm. First results of

the calibration measurement Fig 7b, c showed, that we can reconstruct the position of the transducers to 0.1 mm, if their initial position is within 1mm of the intended position. Furthermore, the individual delays of the electronical channels are corrected. This makes us more independent from the limitations of industrial mass production and reduces the costs.
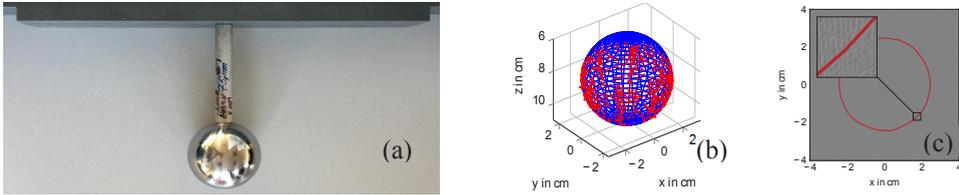
Figure 7: (a) Sphere of 50 mm stainless steel for calibration of our 3D USCTs, (b) first reconstruction of the sphere and (c) by a factor 5 enlarged zone at the surface showing the precision of result.

5   Fast readout electronics

5.1   Integrated TAS electronics via an ASIC

To reduce the costs for the transducer arrays we designed an ASIC, see Fig. 8, which can readout and drive 9 transducers with up to 100 Vpp. The applied technology was AMS 350 nm HVCMOS. By this design, transducers can be operated. One selectable HV amplifier drives the emitter channel, see Fig. 9. The nine receiver preamplifiers are multiplexed to three readout channels. The 3 dB bandwidth of the 3-stage preamplifier is 3 MHz around a middle frequency of 2.5 MHz. The gain can be programmed between 40 and 720. The noise related to the input is ~4 µV, the crosstalk -30 dB.
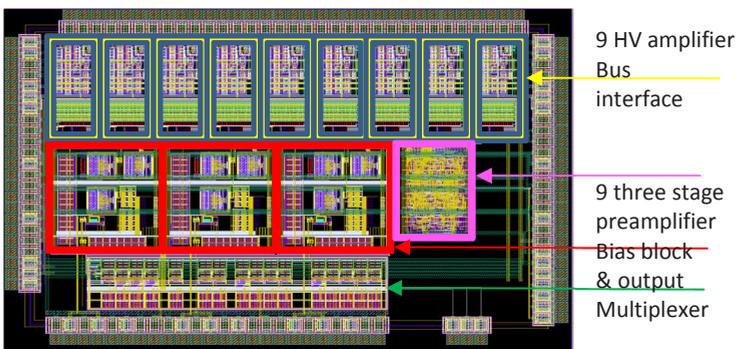
Figure 8: Layout of the ASIC. At the upper side of the ASIC the nine HV amplifier channels could be recognized, well separated to reduce the cross coupling. Below these HV stages are in 3 blocks 3 three stage preamplifier. Bus interface and output multiplexer complete these functions.
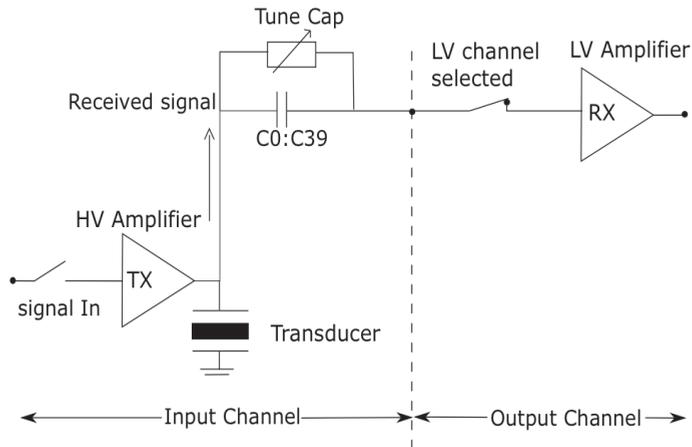
Figure 9: Simplified schematic of the ASIC consisting of high voltage (HV) amplifier and preamplifier (LV).

5.2 Performance increase by a new DAQ hardware

The large number of A-scans (10^7) was obtained in 3D USCT II by 10 motion-steps of the aperture. The DAQ speed for USCT 2.5 was increased by two changes. Firstly, we use a stronger motor for faster movements reducing the DAQ time from 8 to 6 minutes. The use of each transducer as emitter and receiver increases the number of emitters per aperture position and A-scans by a factor two. 3D USCT III will have a factor 1.6 more transducers (128 TAS with 18 transducers each) and therefore will need only two aperture positions to obtain the same number of A-scans as before. The new electronics will reduce the DAQ-time further by a factor of 2 to 2 minutes. Also, the probability for patient movement will be reduced by this factor 5 shorter measuring time.

Our micro-TCA system (Fig. 10) developed in a collaboration with DESY [14] contains a Kintex 7 FPGA from Xilinx which is large enough to do signal preprocessing. That reduces the necessary time of signal processing by nearly two orders of magnitudes by the massive parallel processing in the FPGA. A fast PCI-Express linked to a serial ATA disk reduces the readout time from 15 to 1.5 minutes. The use of a new generation of GPUs accelerate the reconstruction by more than half an hour, so that the total DAQ and reconstruction time shrinks from roughly 2 hours to less than a quarter of an hour, see Tab. 2.
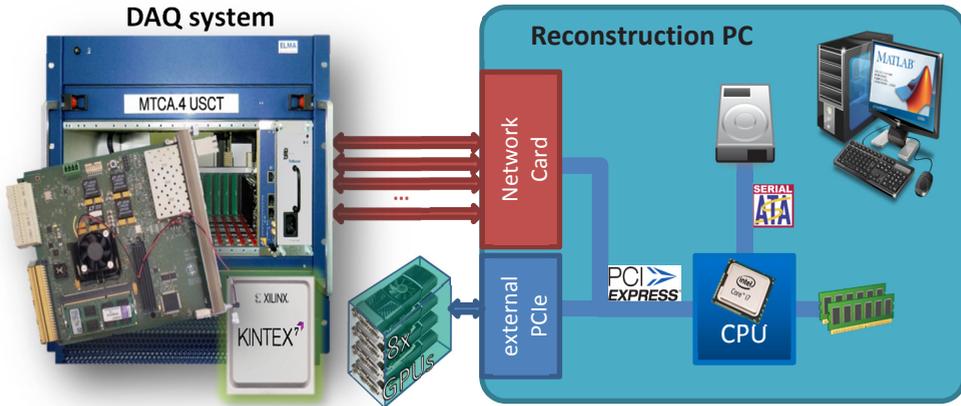
Figure 10: DAQ system and reconstruction PC. The DAQ system is based on a micro TCA system equipped with a Xilinx Kintex 7 FPGA. The reconstruction PC has as support 8 GTX Titan GPUs.

	DAQ	Signal preprocessing	Readout time	TOFI-SAFT	Total
3D USCT II	6 min	Matlab: 55 min	15 min	8 GTX 590: 41min	117 min
3D USCT III	2 min	12 Kintex 7: 2.5 s	1.5 min	8 GTX Titan: 9 min	12.5 min

Table 2: Comparison of 3D USCT II and III in respect to DAQ, signal preprocessing, read out and reconstruction time.

6 Discussion and Conclusion

So far, all known demands of 3D ultrasound tomography are fulfilled to achieve all three modalities reflection-, speed of sound, and attenuation tomography with high image quality. Most of the parts of the new system are ready for assembly. The measuring aperture was enlarged to 36 cm, see Fig. 5, to cover a semi-spherical volume of interest with a diameter of 20 cm. The distribution of transducers over the aperture's surface is homogeneous and random to allow statistical sampling of the volume. The simulations promise an increase of contrast for the reflection tomography of a factor 6 and significant more contrast and visibility for transmission tomography. Especially by the new construction of the lifting mechanism the measuring device can be moved within 5 mm directly to the breast cage. The data acquisition time for 10^7 A-scans will be 2 minutes and the readout will be performed within 1.5 minutes. The ASIC has a bandwidth of 3 MHz and allows reconstruction also at frequencies as low as 0.75 MHz. The total imaging time including DAQ and image processing will shrink from about 2h to 13 minutes.

References

[1] N.V. Ruiter, M. Zapf, R. Dapp, T. Hopp, W.A. Kaiser, H. Gemmeke, "First results of a clinical study with 3D Ultrasound computer tomography", IEEE Ultrasonics Symp., 2013.

[2] P. D. Dragnev, D. A. Legg, and D. W. Townsend, "Discrete logarithmic energy on the sphere". Pacific J. Math. 207 (2002), no. 2, 345–358.

[3] H. Gemmeke, T. Hopp, M. Zapf, C. Kaiser, N.V. Ruiter, "3D ultrasound computer tomography: Hardware setup, reconstruction methods and first clinical results", Nuclear Instr. and Methods in Physics Research, A873 (2017) 59-65.

[4] H. Gemmeke, R. Dapp, T. Hopp, M. Zapf, N.V. Ruiter, "An Improved 3D Ultrasound Computer Tomography System", IEEE Ultrasonics Symposium (IUS), (2014) 1009.

[5] A. Kopmann, T. Bergmann, H. Gemmeke et al.: "FPGA-based DAQ system for multi-channel detectors," *Proc. IEEE NSS,* (2008), Dresden.

[6] M.Zapf, P. Pfistner, C.I. Liberman, "Dice-and-fill single element octagon transducers for next generation 3D USCT", Proceeding of International Workshop on Medical Ultrasound Tomography, 2017, in press.

[7] Henry Cohn and Abhinav Kumar, "Universally optimal distribution of points on spheres", J. Amer. Math. Soc. 20 (2007), no. 1, pp. 99-148.

[8] Patent PCT/EP2015/000369, WO 2015/124301 A1.

[9] Donald E. Knuth, Seminumerical Algorithms, volume 2 of The Art of Computer Programming. Addison-Wesley, 1969.

[10] M. Hardt, "Distributed Simulations for 3D ultrasound computer tomography," PHD-thesis KIT 2012, pp.68-84, AV Akademieverlag Saarbrücken, Germany, ISBN: 978-3-8381-3476-5.

[11] N.V. Ruiter, M. Zapf, T. Hopp, H. Gemmeke, "Experimental evaluation of noise generated by grating lobes for a sparse 3D ultrasound computer tomography system," Proc. SPIE Medical Imaging 2013: Ultrasonic Imaging, Tomography, and Therapy, 2013.

[12] B. Diarra, M. Robini, P. Tortoli C. Cachard, H. Liebgott, "Design of optimal 2D nongrid sparse arrays for medical ultrasound", IEEE Trans Biomed Eng. 2013, 60(11):3093-102.

[13] W. Y. Tan, T. Steiner, N.V. Ruiter, "Upper Bound of Accuracy for Self-Calibration of an 3D Ultrasound Tomography System without Ground Truth", Proceeding of International Workshop on Medical Ultrasound Tomography, 2017, in press.

[14] P. Kaever, M. Balzer, A. Kopmann, M. Zimmer and H. Rongen, The Common Data Acquisition Platform in the Helmholtz Association", Journal of Instrumentation, Volume 12, April 2017.